Interface Engineering Enables Robust ZIF-8/N-$BaTa_2O_6$ Films for CO_2 Photoreduction via Dynamic CO_2 Enrichment-Activation Synergy

Hengtao Fu[1], Huihui Li[1,*], Yicheng Yong, Danfeng Xiao, Yuhua Wang*

National & Local Joint Engineering Laboratory for Optical Conversion Materials and Technology, School of Materials and Energy, Lanzhou University, 222 South Tianshui Road, Lanzhou 730000, PR China

* Corresponding author.
E-mail address: lihh@lzu.edu.cn (H. Li), wyh@lzu.edu.cn (Y. Wang).
[1]Dr. Li and Mr. Fu are co-first authors.

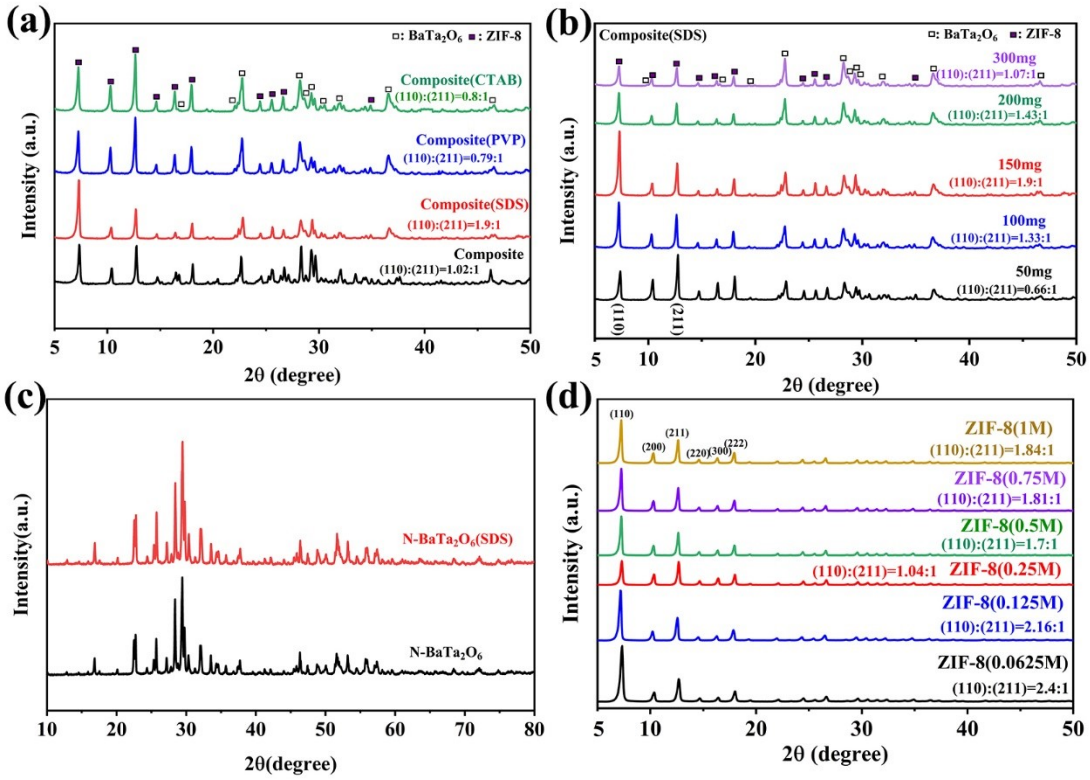

Figure S1. XRD patterns of various samples. (a) Composites synthesized with different surfactant treatments. (b) Composites prepared with different mass ratios of added N-$BaTa_2O_6$. (c) N-$BaTa_2O_6$ before and after SDS treatment. (d) ZIF-8 samples synthesized with different precursor concentrations.

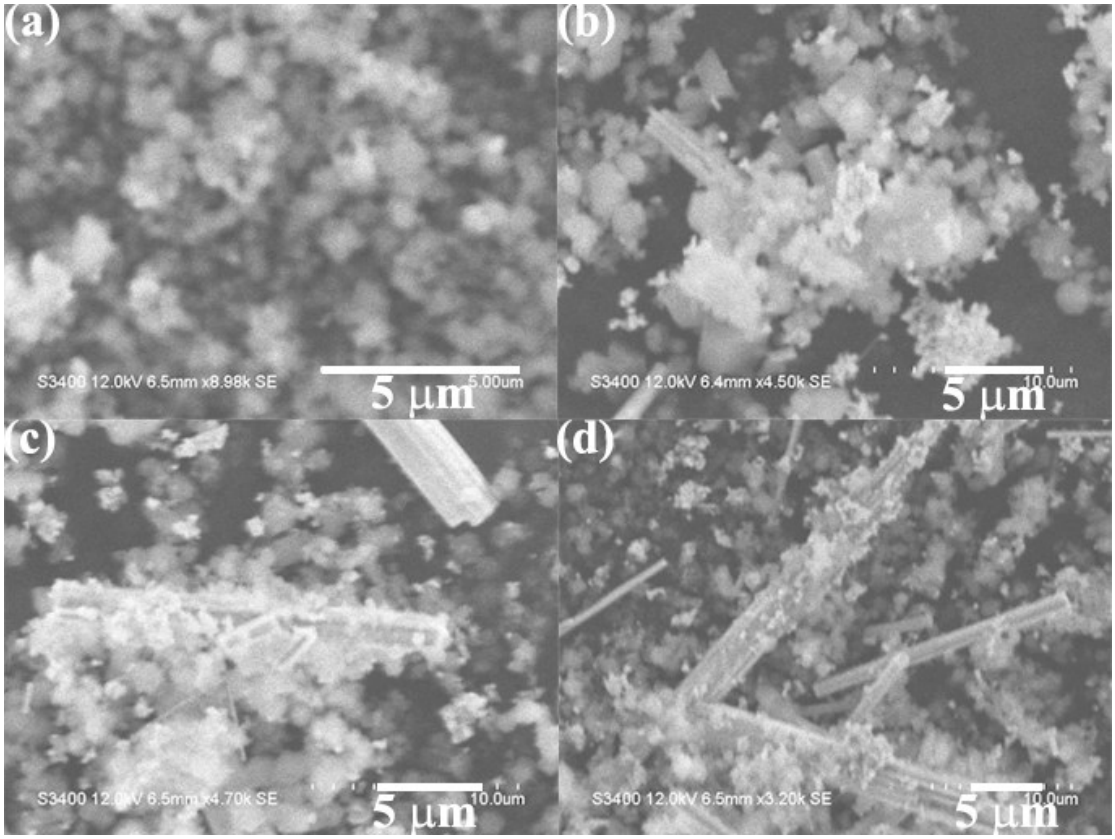

Figure S2. SEM images of composites synthesized with different mass ratios of added N-$BaTa_2O_6$. (a) 50 mg, (b) 100 mg, (c) 200 mg, (d) 400 mg

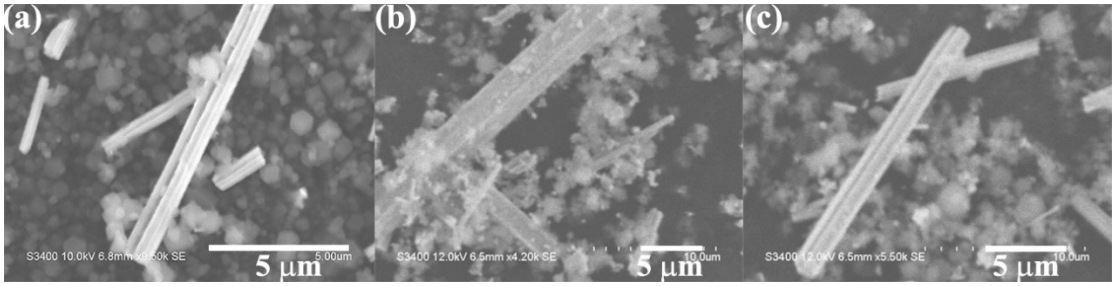

Figure S3. SEM images of composites prepared with different surfactant treatments. (a) Direct hydrothermal synthesis (no surfactant), (b) with CTAB addition, (c) with PVP addition.

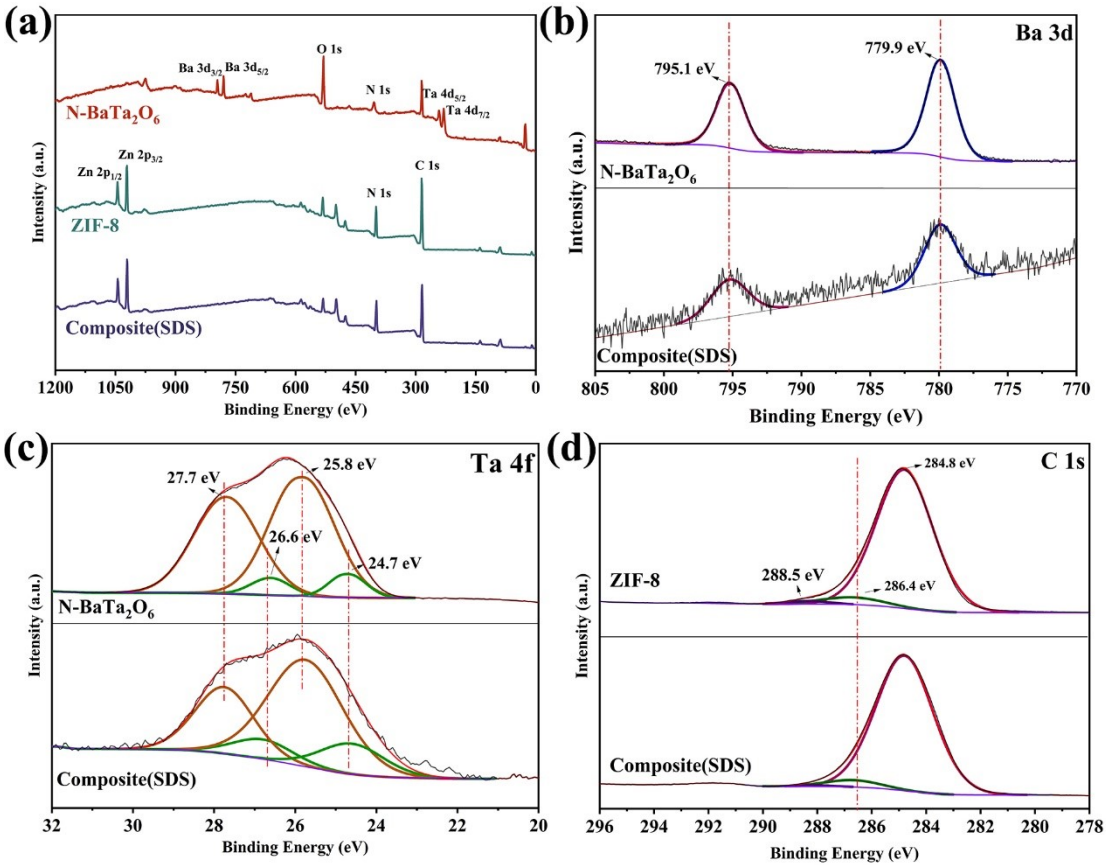

Figure S4. XPS spectra of samples before and after hybridization. (a) Survey spectra of the composite, pristine ZIF-8, and N-$BaTa_2O_6$. (b) Ba 3d spectra of the composite and N-$BaTa_2O_6$. (c) Ta 4f spectra of the composite and N-$BaTa_2O_6$. (d) C 1s spectra of the composite and ZIF-8.

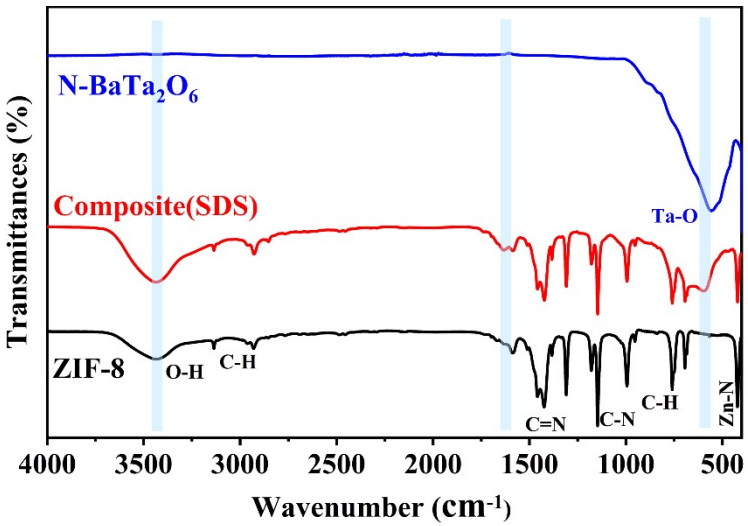

Figure S5. FTIR spectra of the optimal composite (red), pristine ZIF-8 (black) and bare N-$BaTa_2O_6$ (blue).

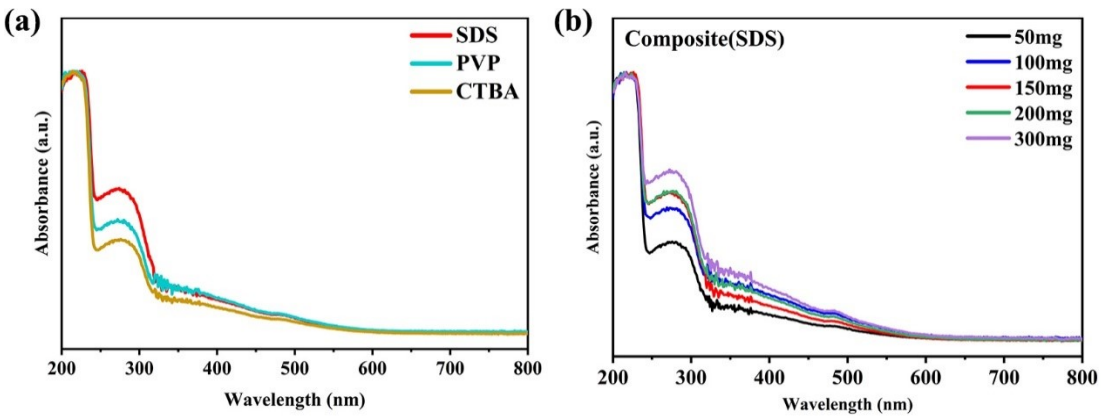

Figure S6. DRS spectra of composites synthesized with (a) different surfactant treatments and (b) different mass ratios of added N-$BaTa_2O_6$.

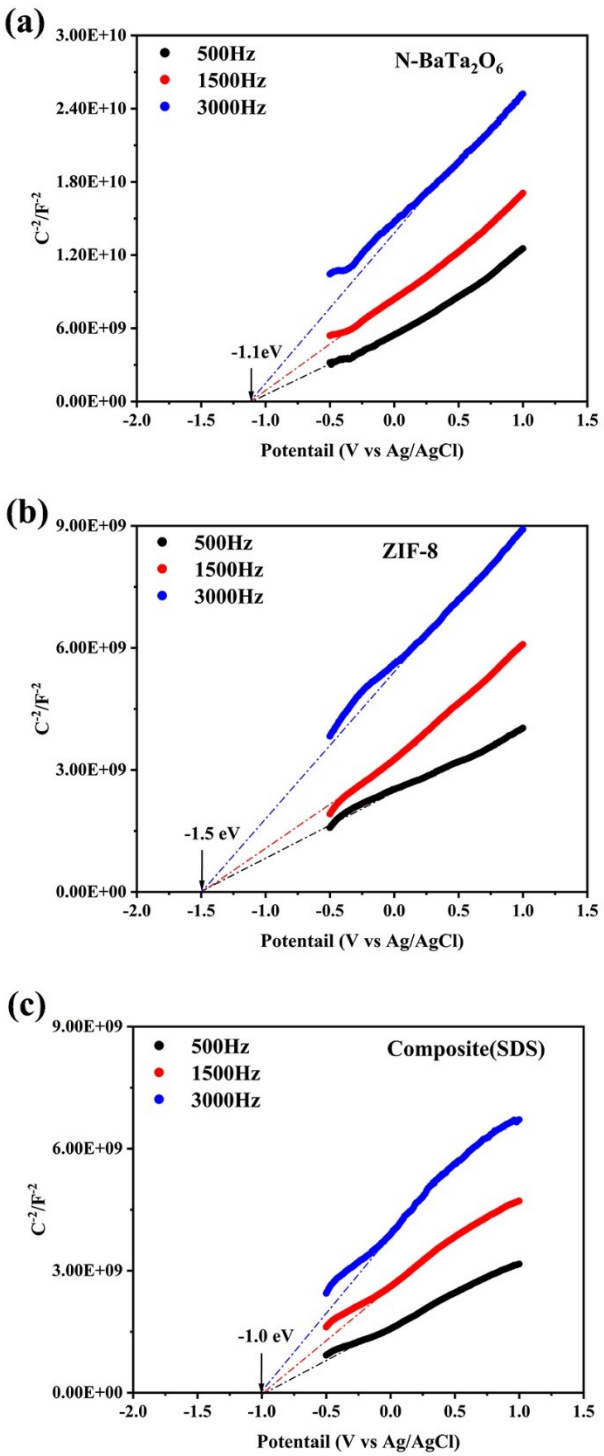

Figure S7. Mott-Schottky plots of (a) N-$BaTa_2O_6$, (b) ZIF-8, and (c) the composite, respectively.

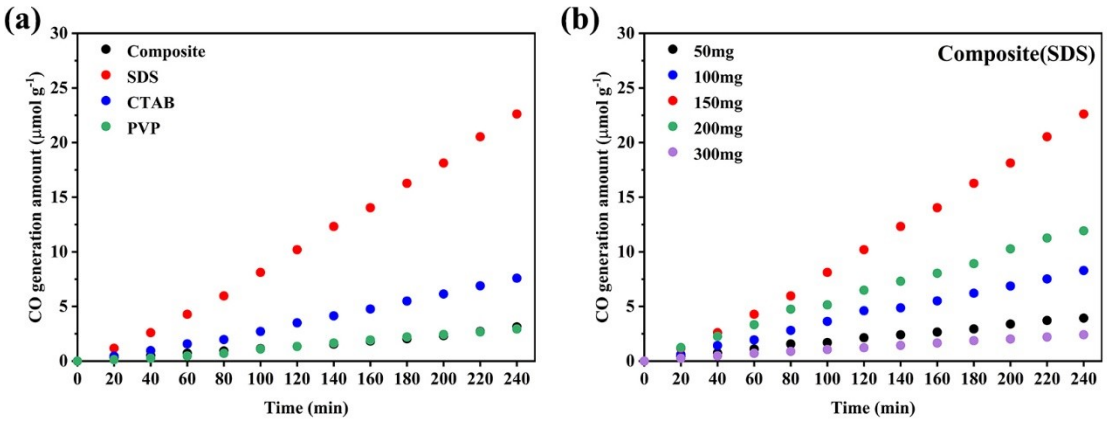

Figure S8. (a) Photocatalytic CO production of composites synthesized with different surfactants (SDS, CTAB, PVP) compared to the direct hydrothermal composite (no surfactant). (b) CO production of composites prepared with different amounts of SDS treated N-$BaTa_2O_6$ in the precursor solution of ZIF-8.

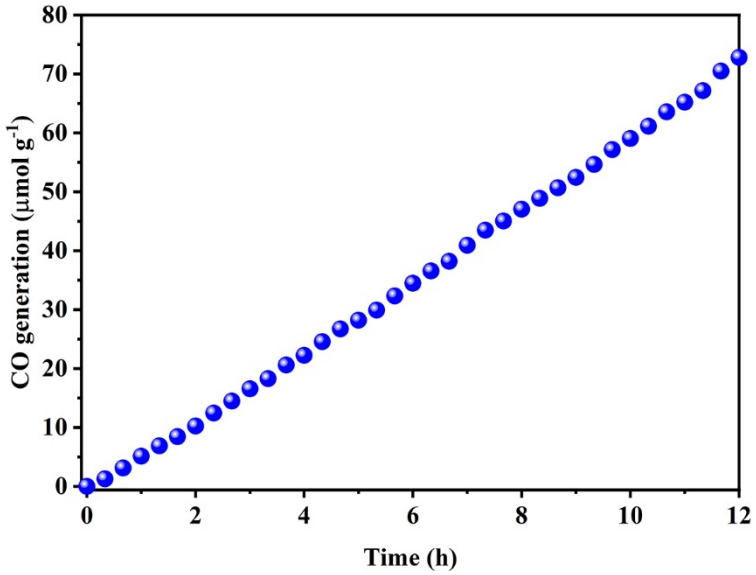

Figure S9. Long-term continuous CO production over the ZIF-8/SDS-N-$BaTa_2O_6$ composite sheet under 12 h of irradiation.

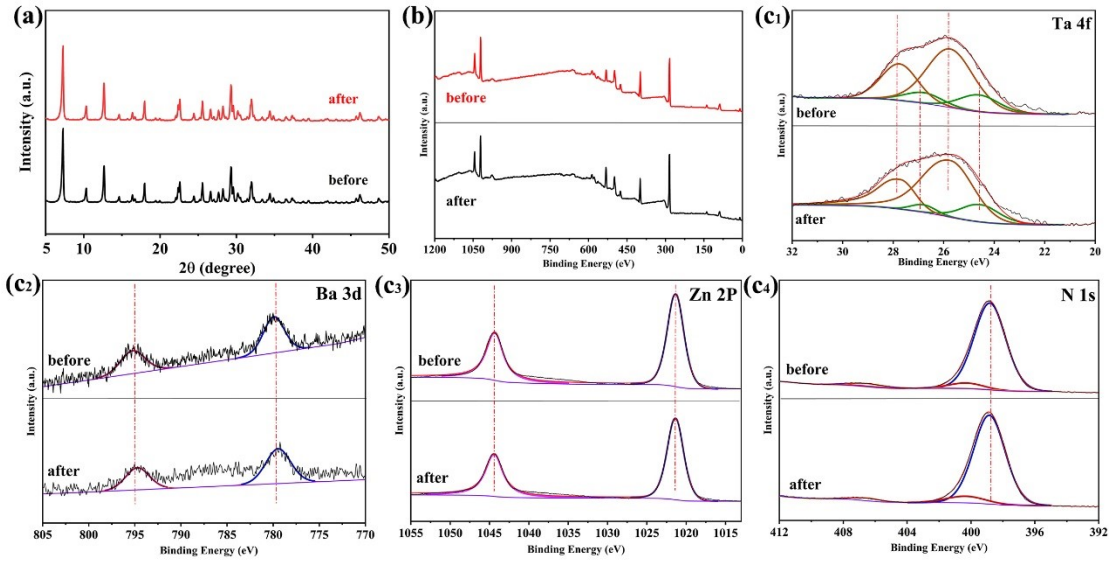

Figure S10. Characterization of the optimal composite before and after photocatalytic reaction. (a) XRD patterns. (b) XPS survey spectra. (c1) XPS Ta 4f spectra. (c2) XPS Ba 3d spectra. (c3) XPS Zn 2p spectra. (c4) XPS N 1s spectra.

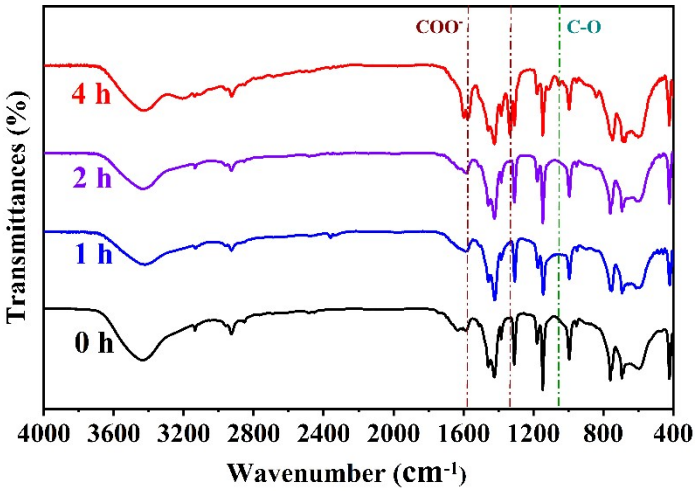

Figure S11. Ex-situ FTIR spectra of the ZIF-8/SDS-N-$BaTa_2O_6$ composite after 0, 1, 2, and 4 h of photocatalytic CO_2 reduction in pure water.

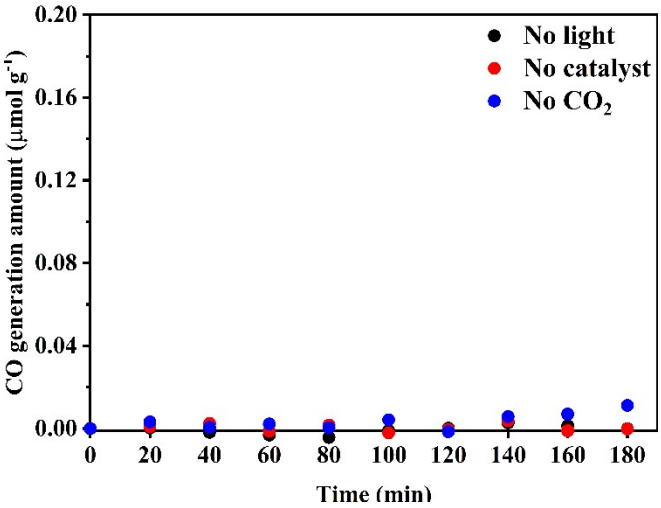

Figure S12. Blank control experiments under different conditions.

Table S1. Conduction band minimum (E_{CB}), valence band maximum (E_{VB}), and band gap (Eg) values for ZIF-8 and N-$BaTa_2O_6$ derived from Mott-Schottky, UPS, and DRS measurements.

Samples	CB (eV)	VB (eV)	Band energy (eV)
ZIF-8	-1.2	2.1	3.3
N-$BaTa_2O_6$	-0.9	1.1	2.0

Table S2. Textural properties of ZIF-8 and the optimal composite determined from N_2 adsorption-desorption isotherms using BET and t-Plot methods: specific surface area (S_{BET}), micropore volume (V_{micro}), and average pore size.

Samples	S_{BET} ($m^2\ g^{-1}$)	S_{mic} ($m^2\ g^{-1}$)	V_{total} ($cm^3\ g^{-1}$)	V_{mic} ($cm^3\ g^{-1}$)	Average Pore Size (nm)
ZIF-8	1830	1837	0.6195	0.6279	1.13
Composite (SDS)	1100	1097	0.3968	0.3737	1.23

Table S3. Relative content (%) of Ta-N and Ta-O species obtained from the deconvolution of XPS Ta 4f spectra for pristine N-$BaTa_2O_6$ subjected to different photocatalytic reaction durations.

Content (%)	Peaks (eV)	before reaction	4h reaction	8h reaction	16h reaction
Ta-N	24.7、26.6	22	8	4	2
Ta-O	25.8、27.7	78	92	96	98

Table S4. Peak area values for the Ta-O, O-H, and C=O species obtained from the deconvolution of XPS O 1s spectra for pristine N-$BaTa_2O_6$ subjected to different photocatalytic reaction durations.

Peak area	Peak (eV)	before reaction	4h reaction	8h reaction	16h reaction
Ta-O	530.0	6139	4926	5355	7139
O-H	531.4	5422	4410	4645	4273
C=O	532.4	0	1623	1950	2157

Table S5. Comparison of photocatalytic CO production rates for representative MOF-oxide composite photocatalysts.

Photocatalyst	Sacrificial agent/photosensitizer	CO generation rate ($\mu mol\ g^{-1}\ h^{-1}$)	Reference No.
ZIF-8/N-$BaTa_2O_6$ (sheet)	-	6.5	Our work
Co-MOF/Cu_2O	-	3.8	S1
Cu_2O/Ni-MOF	-	5.4	S2
UiO-66/$Bi_4O_5Br_2$	-	8.4	S3
MOF-BiOBr/$CdIn_2S_4$	-	3.4	S4
Ce/Zr-NH_2-UiO-66/$CdIn_2S_4$	-	6.0	S5
$NiFe_2O_4$@N/C/SnO_2	TEOA+MeCN+$[Ru(bpy)_3]Cl_2 \cdot 6H_2O$	2057.4	S6
In_2O_3@ZIF-67	TEOA+$[Ru(bpy)_3]Cl_2 \cdot 6H_2O$	33420	S7
PtO/Fe-soc-MOFs	TEOA	56.7	S8
ZIF-67/DCD/Ru	-	1495	S9
Pd-HPP-TiO_2 (sheet)	-	4.9	S10

Reference

S1. D.-S. Li, W.-W. Dong, J. Jia, Y. Wang, J.-R. An, O.-Y. Yang, X.-J. Gao, Y.-L. Liu and J. Zhao, *Chem. Eng. J.*, 2022, **438**, 135622.

S2. H. Jiang, M. Xu, X. Zhao, H. Wang and P. Huo, *J. Environ. Chem. Eng.*, 2023, **11**, 109504.

S3. D. Li, B. Zhu, Z. Sun, Q. Liu, L. Wang and H. Tang, *Front. Chem.*, 2021, **9**, 804204.

S4. M. Shen, Y. Li, T. Luo, Z. Wang, M. Zhou, Y. Wang, S. Xu and Z. Li, *Sep. Purif. Technol.*, 2025, **355**, 129713.

S5. S. Li, H. Li, Y. Wang, Q. Liang, M. Zhou, D. Guo and Z. Li, *Sep. Purif. Technol.*, 2024, **333**, 125994.

S6. W. Zhang, Y. Yu, R. Huang and X. Shi, *ACS Appl. Mater. Interfaces*, 2021, **13**, 40571–40581.

S7. Y.-J. Wang, B. He, D. Ma, R. Li, Y. Xie and J.-R. Li, *Chem. Eng. J.*, 2023, **467**, 143329.

S8. X.-Y. Zhang, P. Wang, X.-Y. Lu, Y. Zhang and W.-Y. Sun, *Chem. Eng. J.*, 2023, **476**, 146560.

S9. F. Dai, M. Zhang, Q. Chen, M. Mi, Z. Li, J. Han, J. Xing, S. Feng and L. Wang, *Appl. Catal. B Environ.*, 2023, **336**, 122934.

S10. Y. Ma, X. Yi, S. Wang, T. Li, B. Tan, C. Chen, T. Majima, E. R. Waclawik, H. Zhu and J. Wang, *Nat. Commun.*, 2022, **13**, 1400.